Nanomed Res J 10(3):258-280, Summer 2025

RESEARCH ARTICLE

Modified Carboxymethyl Cellulose Containing Imine/Chitosan/ Nanoparticles: Synthesis and Study Biological Applications

Huda H. Saeed[1], Ruwaidah S. Saeed[1*], Lyazzat Bekbayeva[2]

[1] Department of Chemistry, College of Education for Pure Science Ibn Al-Haitham/University of Baghdad, Iraq

[2] National Nanotechnology Open Laboratory, Al-Farabi Kazakh National University, Republic of Kazakhstan

ARTICLE INFO

Article History:
Received 26 Apr 2025
Accepted 03 Jun 2025
Published 01 Sep 2025

Keywords:
Antioxidant
Magnesium Oxide Nanoparticles
Nanocomposites
Doxorubicin Drug
Molecular docking
Brain cancer cell line (A172)
Modified CMC/CS

ABSTRACT

The research deals synthesis of new organic compounds containing imine group and then modifying carboxymethyl cellulose (CMC) by reacting carboxymethyl cellulose with the prepared imine compounds and then mixing them with chitosan (CS) and nanoparticles (NPs) such as gold nanoparticles (AuNPs), magnesium oxide nanoparticles (MgONPs) and silver nanoparticles (AgNPs) and studying their important uses in biomedical fields. These prepared nanocomposites (modified CMC/CS/NPs) studied of antibacterial, anticancer and antioxidant activities. The toxicity of the nanocomposites was studied on mice, and histological analysis was performed in vitro. The results indicated that these nanocomposites had a larger diameter of growth inhibition zone compared to standard antibiotics (amoxicillin and tetracycline) and the antioxidant activity of modified CMC/CS/NPs showed a high inhibition rate compared to standard ascorbic acid. The nanocomposites showed excellent inhibition rates and were non-toxic against anticancer cells (A172), and compared to the normal cell line (REF). Molecular docking is used to determine the binding of the compounds to the enzyme and to determine the free energy (ΔG) of the synthesized compounds, so that they can be compared to the drug doxorubicin, making them useful in pharmaceutical manufacturing. Using H-NMR spectroscopy, FTIR, Transmission Electron Microscopy (TEM) and Field Emission Scanning Electron Microscopy (FESEM) the synthesized compounds were characterized.

How to cite this article
H.Saeed H., S.Saeed R., Bekbayeva L. Modified Carboxymethyl Cellulose Containing Imine/Chitosan/ Nanoparticles: Synthesis and Study Biological Applications. Nanomed Res J, 2025; 10(3): 258-280. DOI: 10.22034/nmrj.2025.03.006

INTRODUCTION

Carboxymethylcellulose (CMC) is an anionic natural polysaccharide. Carboxymethyl cellulose (CMC) possesses numerous compelling attributes as a polymer. It has high chemical stability, good solubility, and is non-toxic [1-4]. Furthermore, it is a biodegradable and cost-effective polymer suitable for biocompatibility and film production [5-7]. The pharmaceutical, food, and packaging sectors utilize it widely due to its safety and nontoxicity [8]. Conversely, carboxymethyl cellulose (CMC) is readily amenable to chemical modification and is utilized in various applications due to its abundant hydroxyl and carboxyl groups, as well as its environmental compatibility [9-13]. Pure CMC films readily dissolve in distilled water, necessitating the incorporation of other ingredients for various uses [14,15]. When CMC is combined with other consumable substances (such as CS) [16-19]. Chitosan is a natural polymer derived from the alkaline deacetylation of chitin, a structural component of the exoskeletons of crustaceans such as crabs and prawns [20,21]. Chitosan is the second most abundant organic substance in nature, following cellulose. Chitosan is a weak base that is insoluble in water [22]. This phenomenon is likely attributable to the existence of robust intermolecular hydrogen bonds generated between the molecular chains of chitosan [23]. However, it can dissolve in weak acidic water with a pH below 7, where it changes glucosamine units ($-NH_2$) into a form that can dissolve better (NH_3^+). The solubility of chitosan is contingent upon its

* Corresponding Author Email: *ruaida.s.s@ihcoedu.uobaghdad.edu.iq*

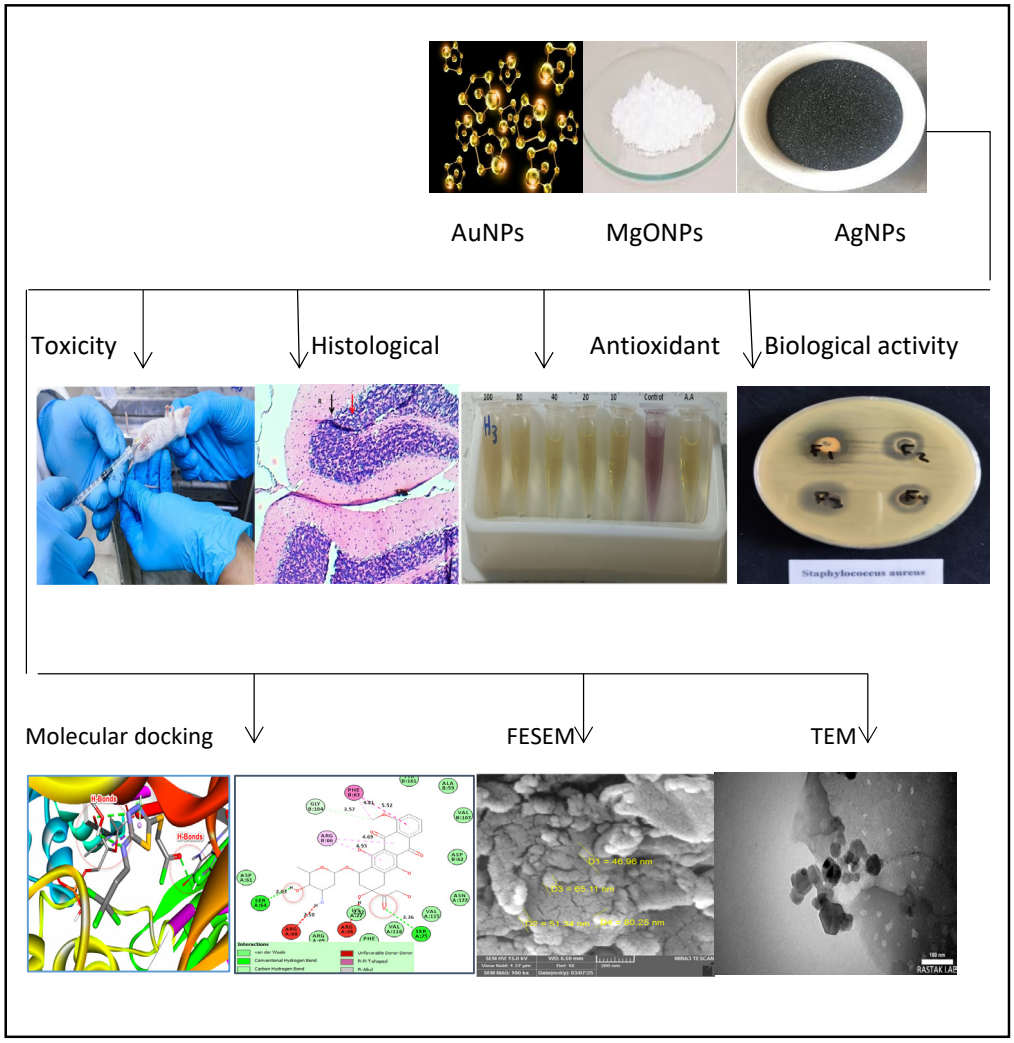

Scheme 1. Summarizes all the work for the current project.

natural origin, molecular weight, and degree of deacetylation [24]. Chitosan is a robust polymer. because its molecules have hydrogen bonds. Chitosan is special because it is plentiful, can be modified on its surface, and has unique properties such as being biodegradable, biocompatible, non-toxic, antibacterial, hydrophilic, mucoadhesive, and having anticholesterolemic actions [25,26]. Chitosan is a very useful molecule that may be used in many different ways, such as in medicine, farming, food preservation, biocatalysis, and the environment [27]. Because it has amino and hydroxyl groups, chitosan does not have anionic characteristics. Biopolymer-based nanocomposites have rapidly emerged in recent years [28]. Researchers are currently looking at how to combine nanomaterials (NMs) with biodegradable polymers. Polysaccharides are safe for living things, break down quickly, and are quite common [29,30]. Polysaccharides are widely used to reduce and stabilize metal nanoparticles (MNPs) because they are good for the environment and easy to convert into different types of hydrogels [31]. Nanoparticles (NPs) make biopolymers better at blocking heat, mechanical stress, biological activity, and other things, which makes them more useful [32]. T h e present study to synthesize new series of imine compounds then modified carboxymethyl cellulose with imine prepared compounds and blending with chitosan , nanoparticles with screened of antibacterial , antioxidant and anticancer activities. Based on these preliminary theoretical

and experimental results, these novel species have potential as drug candidates, and future work will involve in vivo studies.

MATERIALS AND METHODS

Materials

AuNPs or MgONPs or AgNPs were supplied by US, Research Nanomaterials, Inc. Chemicals have been provided from BDH and CDH

Instrumentation

With a range of 400 cm^{-1} to 4000 cm^{-1}, the Shimadzu FT-IR-8400S was used to record the FT-IR spectra. Ultra Shield 400 MHz, manufactured by Bruker, University of Tehran, Iran, was used to perform the ^{1}H-NMR spectra. As an internal standard, TMS has been used using DMSO as the solvent. The University of Tehran in Iran was the site of the field emission scanning electron microscopy (FESEM) study. To visualize ligands, proteins, hydrogen bonding interactions, short contacts, and bond length measurements, molecular docking was carried out using the CCDC Hermes visualizer program (version 1.10.3). Biological activity took place at the University of Baghdad's Central Environmental Laboratory, College of Science. Perform an acute toxicity test in the lab of the Centre for Cancer Research and Medical Genetics.

Synthesis of 2-amino-5-mercapato-1,3,4-thiadiazole[33]

This compound was synthesized in accordance with the literature (Ali H.Samir et.al. 2014). The M.P. (229-231) C° and the FTIR spectrum were in agreement with the literatures

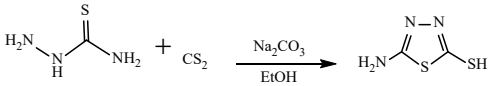

Synthesis of compounds [I-VI][34]

2- amino-5- mercapto -1,3,4 - thiadiazole (1.33 gm.,0.01mol) or 4-amino benzene thiol (1.25gm.,0.01mol) mixed with(0.01mol) of trichloro propanal or 2,4-dichloro benzaldehyde or syringaldehyde in 20ml of absolute ethanol with three drops of glacial acetic acid, the mixture was refluxing at(75-80) C° for 14h.The reaction mixture was cooled, the precipitate filtration and recrystallized from ethyl acetate to give:(Pale yellow, (248-250 (C°, yield65%) ,(Very light brown, (137-138)C°, 72%),(Yellow,254-256C°, 96%), (Dark yellow, 229-230 C°, 70%), (Yellow green,158-160C°,81%),(Yellow green, 240-242C°, 54%) respectively. Scheme 2. shows the formation steps of compounds [I-VI]

Synthesis of compounds [VII-XII] [35]

Aliquot (0.01mol) one of the compounds [I-VI] mixed with (0.02 mol) anhydrous sodium carbonate in (15ml) distilled water then (0.01mol) of chloroacetic acid was added. The solution refluxed for 6h. then added conc. hydrochloric acid to reached out pH= 2. Filtered the product and washed with distilled water and recrystallized from absolute ethanol to produce: (Yellow, 187-189C°, 97%), (very light brown,228-230C°,78%), (Yellow,179-180C°, 82%), (White,193-195C°,78%), (White,164-165C°,75%), (Orange, 250-251C°, 90%) respectively. Scheme 2 shows the formation steps of compounds[VII-XII]

Synthesis of compounds [XIII-XVIII] [36]

(0.01mol) of one of the compounds [VII-XII] mixed with $SOCl_2$ (0.01mol) in 15ml dry benzene was refluxed for (8 h.) The excess of thionyl chloride and benzene were outlying under vacuum. (Dark brown,160-162C°, 93%) (Dark orange,239-241C°,96%), (Dark brown, 118-120C° ,94%), (Dark indigo,183-185C°,69%), (Red, >300 C°, 63%), (Brown,210-212C°, 92%) respectively. Scheme 2. shows the formation steps of compounds[XIII-XVIII]

Synthesis of Modified CMC [XIX-XXX] [37]

Modified CMC [XIX-XXX] has been prepared by the reaction (0.1gm.) of one compounds [XIII-XVIII] with 0.1 gm. of CMC in 20 ml of DMF, the mixture was refluxed for 8 h. The solution was poured on a Petri dish and left to dry at room temperature. shown in Scheme 3 and Scheme 4

Synthesis of Blend Polymers [XXXI-XLII] [38]

Solvent casting was employed to create polymer blends. One of modified CMC [XIX-XXX] was dissolved in water and stirred for 1 hour at room temperature to create the modified CMC [XIX-XXX] solutions, 1 gm of chitosan dissolved in (49 mL of 2% percent aqueous acetic acid solution) and stirring for 1 hour at room temperature to create the chitosan solutions. Two polymer solutions (CMC solutions and Chitosan solutions) were mixed to prepare homogenous solution by using hotplate stirrer for 60 min after the two polymers' solutions had been combined. The modified CMC/CS blends were created by combining Modified

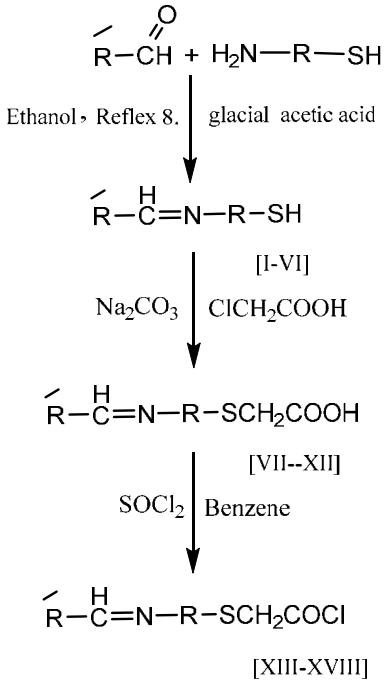

Scheme 2. Synthesis of compounds [I-XVIII]

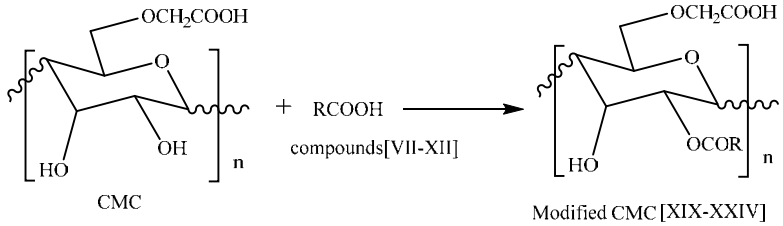

Scheme 3. Synthesis of modified CMC [XIX-XXIV]

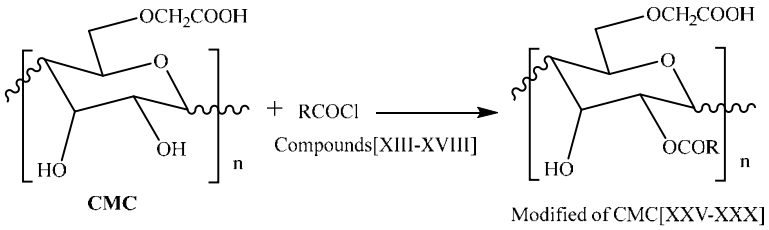

Scheme4. Synthesis of modified CMC[XXV-XXX]

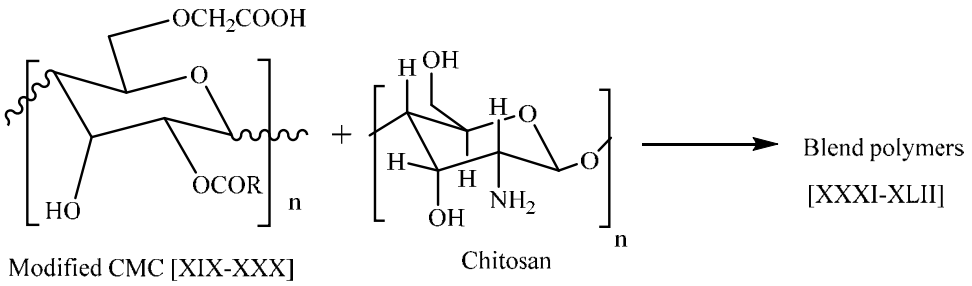

Scheme 5. Synthesis of blend polymers [XXXI-XLII]

Scheme 6. Synthesis of Nanocomposites [XLIII-LX]

Table 1. FT-IR spectroscopy data of compounds [I-VI]

Comp. No.	(S-H) cm^{-1}	=C-H arom.	(C=N)	(C=N) of thiadiazole	(C=C)	(C-S)
[I]	2360	3099	1653	1607	1590	642
[II]	2525	3029	1673	1625	1588	645
[III]	2325	3010	1606	1669	1585	632
[IV]	2380	3110	1607	-	1590	671
[V]	2350	3062	1630	-	1581	675
[VI]	2370	3032	1640	-	1585	631

CMC: CS (5:5) in one ratio. shown in Scheme 5.

Synthesis of Nanocomposites (Modified CMC/CS / Nanoparticles)[XLIII-LX] [39]

In order to bond the gold, or magnesium or silver nanometals in the blend matrix, 100mg of the dried modified CMC/CS [XXII-XXVII] was added to 50mL of AuNPs or MgONPs or AgNPs solution of a 250 mg/L concentration. This was done with the use of a hotplate stirrer for three hours. shown in Scheme 6

RESULTS AND DISCUSSION

FTIR and ^{1}HNMR of Synthesis Compounds

Scheme (1) illustrates the process of synthesizing new compounds from Schiff bases. The compounds [I-VI] are synthesized by combining 2-amino-5-mercapto-1,3,4-thiadiazole or 4-amino benzene thiol with various aldehydes in ethanol and heating the mixture for 14 hours The FTIR spectra of compound [VI] exhibited peaks at 2325, 1640cm^{-1}. these peaks are linked to the SH group and C=N, respectively, Table 1. Show FT-IR data of compounds [I-VI] . ^{1}H-NMR of compound [VI] showed a singlet at δ3.36 ppm for the proton of SH , doublets at 4.59–4.76 ppm for 2(OCH_3), a singlet at δ5.06 ppm for the proton of OH, an extra signal at δ9.82 ppm for the proton of CH-N, and several peaks at δ6.50–7.73 ppm for aromatic protons. The reaction of compounds [I-VI] with chloroacetic acid in distilled water produced compounds [VII-XII] in a basic environment. The FTIR. spectra of compound [XII] show peaks for the hydroxyl group at 3400–2400 cm^{-1} and for the carboxylic group at 1680 cm^{-1}, Table 2. shows FT-IR of compounds[VII-XII] . ^{1}H-NMR of [XII] showed a singlet signal at a chemical shift of δ 13.21 ppm, which was caused by carboxylic proton. There was a signal at δ 9.78 ppm that had to do with the proton of CH-N. There were several peaks in the region of δ 7.12–7.77 ppm for aromatic protons, as well as a single signal at δ 3.85 that

Table 2. FT-IR spectroscopy data of compounds [VII-XII]

Comp. No.	(O-H)cm^{-1}	(C-H) arom. cm^{-1}	(C=O) carboxlic	(C=N) of thiadiazole	(C=N)cm^{-1}	C=C)
[VII]	3400-2400	3057	1693	1631	1654	1572
[VIII]	3400-2400	3000	1692	1628	1650	1600
[IX]	3400-2400	3004	1695	1664	1605	1581
[X]	3400-2400	3093	1686	-	1606	1588
[XI]	3400-2400	3044	1683	-	1651	1601
[XII]	3400-2400	3049	1680	-	1627	1592

Table 3. FT-IR spectroscopy data of compounds [XIII-XVIII]

Comp. No.	(C-H) arom. cm^{-1}	(C=O)-Cl	(C=N)	(C=N) of thiadiazole	(C=C)	(C-S)
[XIII]	3037	1740	1651	1622	1572	680
[XIV]	3047	1746	1650	1604	1578	662
[XV]	3047	1746	1651	1605	1592	662
[XVI]	3037	1710	1622	-	1572	675
[XVII]	3039	1770	1651	-	1595	661
[XVIII]	3066	1740	1607	-	1582	674

Table 4. FT-IR data of polymers[XIX-XXX]

Com. No.	(O-H)cm^{-1}	(C-H) aliph. cm^{-1}	(C=O) ester.cm^{-1}	(C=N) cm^{-1}	(C=C) cm^{-1}	(C-O-C) cm^{-1}
[XIX]	3251	2920,2869	1709	1645	1584	1018
[XX]	3310	2918,2880	1733	1650	1592	1017
[XXI]	3257	2924,2884	1710	1624	1592	1020
[XXII]	3337	2924,2869	1723	1653	1589	1017
[XXIII]	3231	2996,2885	1734	1647	1561	1056
[XXIV]	3353	2918,2884	1740	1678	1591	1017
[XXV]	3267	2924,2881	1710	1641	1590	1024
[XXVI]	3296	2922,2886	1710	1640	1591	1018
[XXVII]	3340	2943,2881	1716	1634	1595	1060
[XXVIII]	3271	2927,2879	1716	1630	1590	1051
[XXIX]	3275	2924,2900	1731	1650	1595	1017
[XXX]	3288	2922,2877	1736	1628	1571	1020

corresponded to two protons of S-CH_2. There were doublet indications at 3.76–3.77 ppm for 2(OCH_3). When the synthesized chemicals [VII-XII] were mixed with $SOCl_2$ in dry benzene, they made many derivatives[XIII-XVIII]. The FTIR analysis of the compound[XVIII] shows disappearance band at 3400–2400 cm^{-1}, which is linked to the (OH) group of the carboxylic acid. Instead, there is a band at 1740 cm^{-1}, which indicates the acyl chloride, Table 3. FT-IR spectroscopy of compounds [XIII-XVIII].

CMC derivatives [XIX-XXX] were prepared through the reaction between [VII-XVIII] with the CMC in DMF as the solvent. The FT-IR spectrum of the polymer [XXIX] illustrated a large peak at 3275 cm^{-1}, which indicates the hydrogen bonding OH stretching region. The small hump at 29224cm and 2900 cm^{-1} shows the attributable C-H stretching vibration. The sharp peak observed at 1731 cm^{-1} confirms the presence of C=O, which is assigned to the stretching of the ester group, Table 4 FT-IR data of polymers[XIX-XXX]. ^{1}H-NMR spectrum of modified CMC[XXIX], singlet signal with a chemical shift at δ 12.6 ppm as a result of the proton of carboxylic protons, additional signal at δ δ8.87 ppm due to the presence of protons for CH-N, multiple peaks appeared at δ δ7.01-8.00ppm for aromatic protons, and a singlet signal at δ 3.85 for two protons for the S-CH_2, The characteristic peak

Table 5. FT-IR data of polymers [XXXI-XLII]

Com. No.	υ (O-H) and (N-H)	υ (C-H) aliph. cm^{-1}	υ (C=O) ester. cm^{-1}	υ (C=C) cm^{-1}	υ (C=N) cm^{-1}	υ (C-O-C) cm^{-1}
[XXXI]	3359	2917,2874	1701	1600	1648	1056
[XXXII]	3257	2918-2851	1720	1571	1620	1061
[XXXIII]	3339	2920, 2874	1740	1556	1631	1058
[XXXIV]	3287	2910,2861	1701	1551	1648	1061
[XXXV]	3340	2925,2882	1714	1584	1625	1060
[XXXVI]	3247	2920,2885	1710	1588	1620	1048
[XXXVII]	3281	2918,2897	1716	1592	1630	1051
[XXXVIII]	3268	2920,2855	1730	1579	1628	1054
[XXXIX]	3349	2915,2877	1710	1556	1648	1056
[XL]	3280	2924,2870	1711	1590	1650	1054
[XLI]	3303	2933,2885	1710	1598	1650	1060
[XLII]	3329	2921,2880	1712	1588	1612	1050

of CH_2COOH on C_6 of CMC is near 4.27-4.64, signals at 2.10-2.26 (H_2, H_3, H_4, H_5) of CMC, signals at 4.66-4.81 due to H_1 of CMC, signals at 6.98 for OH of CMC, and signals at 12.6 due to CH_2COOH on C_6 of CMC . ^{1}H-NMR spectrum of modified CMC[XXX], singlet signal with a chemical shift at δ 11.82 ppm as a result of the proton of carboxylic proton on C6 of CMC, additional signal at δ9.70 ppm due to the presence of proton for CH-N, multiple peaks appeared at δ7.23-8.27ppm for aromatic protons , a singlet signal at δ5.96 ppm due to presence of proton for OH singlet signal at δ3.85 for two protons for the S-CH_2 , doublet signals at 2.98-3.07ppm at 2(OCH_3) ,The characteristic peak of CH_2COOH on C6 of CMC is near 4.27- 4.64, signals at 2.10-2.36 of (H2,H3,H4,H5) of CMC, signals at 4.66-4.81 due to H1 of CMC , signals at 5.96 for OH of CMC. Modified CMC Blended with CS to prepare a blend, polymer research of the characteristics of the obtained blends had shown a good level of miscibility between the CMC and CS that had been shown by FT-IR results of the blend polymer[XLII], the band broadening in the (2400-3600) cm^{-1} region because of a strong intermolecular bonding of hydrogen that exists between amino groups of CS and CMC's hydroxyl groups, and 1612 cm^{-1} as a result of (C=N) and 1712 cm^{-1} cm^{-1}due to carbonyl of ester,Table 5.FT-IR data of polymers[XXXI-XLII].The preparation of nanocomposites[XLIII-LX] using blend polymers [XXXIV-XXXIX] with AuNPs, MgONPs, and AgNPs. FT-IR data of nanocomposites [XLIII] shows that the presence of peaks at 3288 cm^{-1} reveals O-H stretching from the inter- and intra-molecular hydrogen bonds and shifting asymmetric and symmetric stretching vibrational of C-H from alkyl groups at (2861, 2920) and 400 to 800 cm^{-1} of (Au, MgO, Ag) NPs bonding also supports the formation of particles.

Field Emission Scanning electron microscope studies (FESEM) [40,41]

The FESEM approach reveals that the surface morphology differs for the Modified CMC blend with CS [XXV] (Fig.1), Modified CMC/CS/AuNPs [XLIII] (Fig.2), Modified CMC/CS/MgONPs [XLIV] (Fig.3) and Modified CMC/CS/AgNPs [XLV] (Fig. 4). The incorporation of CS modifies the surface topography of the composite membrane and significantly influences cell spreading. The FESEM image indicates a homogeneous dispersion of nanoparticles (NPs) on the matrix surface. The average particle size of the modified CMC blend with CS [XXV] ranges from 428 to 532 nm in the presence of CS. The average particle size of modified CMC/CS/Ag ranges from 34 to 79 nm, while that of modified CMC/CS/MgO ranges from 46 to 80 nm. The average nanoparticle size for gold nanoparticles is between 24 and 33 nm, which exhibit a homogeneous distribution on the matrix surface. The particles in the nanocomposite film exhibited an almost spherical shape. Nevertheless, certain clusters of nanoparticles were observed, and the surface exhibited a degree of roughness. The nanoparticles displayed a uniform dispersion in CMC/CS and a robust attachment to the polymer. The nanoparticles did not exhibit any significant cytotoxic effects on human cells. The coating on the nanoparticle surface might help reduce harmful effects or completely prevent toxicity.

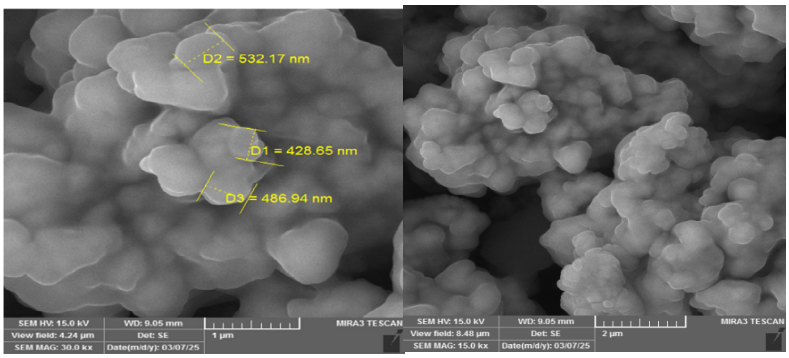

Fig. 1. FESEM of modified CMC/CS[XXV]

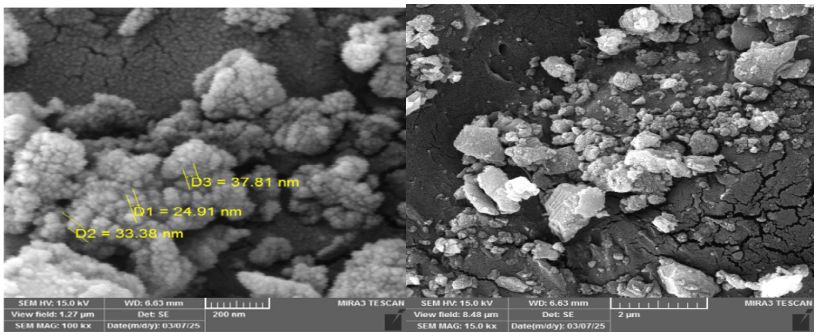

Fig. 2. FESEM of modified CMC/CS/AuNPs[XLIII]

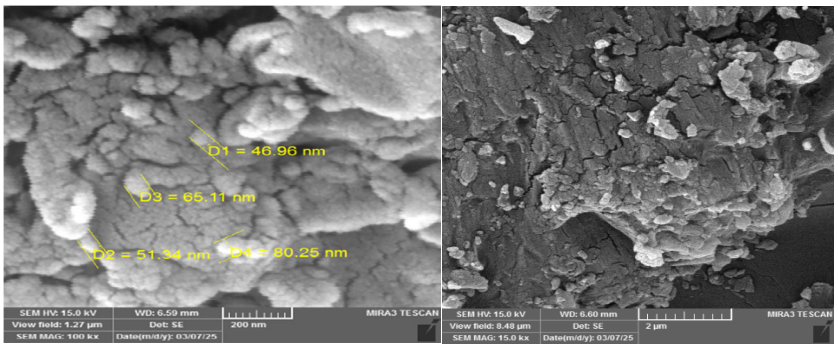

Fig. 3. FESEM of modified CMC/CS/MgONPs [XLIV]

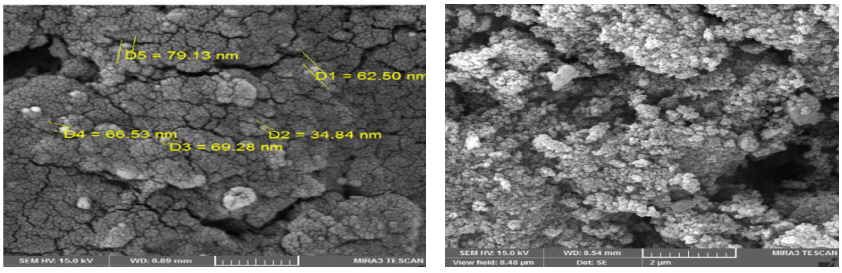

Fig. 4. FESEM of modified CMC/CS/AgNPs[XLV]

Transmission Electron Microscopy (TEM) [42,43]

The TEM picture of the modified CMC/CS suspension drop-cast with AuNPs or AgNPs reveals that the AuNPs or AgNPs are uniformly disseminated and exhibit a semi-spherical morphology. Despite the differing orientations of the particles and their closed nature, there are no indications of agglomeration. The AuNPs or AgNPs generated in the improved CMC/CS exhibit enhanced stability. The TEM picture revealed that the synthesized modified CMC/CS/AuNPs [XLIII] and modified CMC/CS/AgNPs [XLV] were semi-spherical, with dimensions ranging from 50 to 100 nm, as illustrated in Figs 5 and 6. The particles exhibited a spherical morphology, encased in a thin layer of gold or silver around modified CMC/CS.TEM micrographs revealed homogeneous layers of gold or magnesium nanostructures enveloping the modified CMC/CS. The altered CMC/CS seemed to be enveloped in a coating of gold or silver particles, confirming the formation of CMC/CS/AuNPs and CMC/CS/AgNPs.

Molecular docking Study [44,45]

Molecular docking Study Molecular docking for compounds [XII-XIV] is studied, where operations are used to predict the binding status of compounds with the enzyme and to calculate the free energy (ΔG) of the compounds prepared with the human topoisomerase II alpha, which was chosen to perform the molecular docking of the derivatives, as this enzyme plays an important role in cell replication and division, and its inhibition reduces or inhibits the process of non-programmed cell division (cancer cells). The enzyme with the symbol (PDB:ID:5GWK) was chosen; its dimensions were (40, 40, 40) (X, Y, Z), and its location coordinates were (36.578, -24.476, 39.415) (X, Y, Z), and the following figures 7-10 and Table 6 show the interaction between the protein and these compounds.

Molecular docking studies showed the interference of doxorubicin with the binding site of the protein at the docking point value -9.0 kcal/mol and at the conformational value (RMSD.i.b(3.031 RMSD.u.b(8.702)) with the presence of two hydrogen bonds between the amino acid residues SER:A:64, the OH group in the compound, and the hydrogen bond between the amino acid residues. SER: A:75 with the C=O group in the drug show Fig.7.

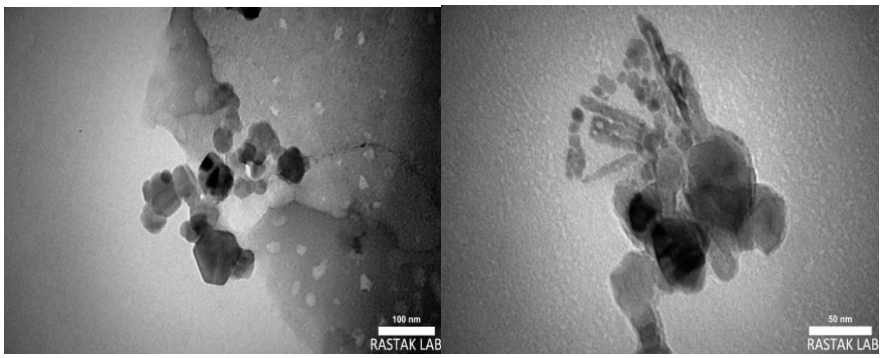

Fig. 5.TEM of modified CMC/CS/AuNPs [XLIII]

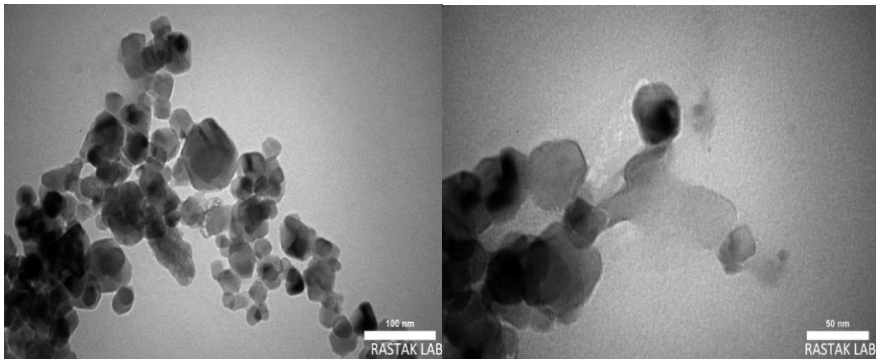

Fig. 6. TEM of modified CMC/CS/AgNPs [XLV]

Table 6. Results of molecular docking of compounds [XII-XIV] via the human topoisomerase II alpha enzyme

Comp. No.	Affinity (Kcal/mol)	RMSD l.b. (A°)	RMSD u.b. (A°)	Distance (A°)	Main residue	Type of Interaction
[XII]	-9.5	1.493	1.911	2.66983	A:LEU616:HN - :UNK1:O	Conventional Hydrogen Bond
				2.0025	A:GLY617:HN - :UNK1:O	Conventional Hydrogen Bond
				3.02046	F:DG13:H1 - :UNK1:O	Conventional Hydrogen Bond
				1.9464	:UNK1:H - A:ASP541:OD2	Conventional Hydrogen Bond
				3.45931	:UNK1:C - A:ARG487:O	Carbon Hydrogen Bond
				3.49741	:UNK1:C - D:DT9	Pi-Sigma
				3.84466	C:DC8 - :UNK1	Pi-Pi Stacked
				4.48912	:UNK1:C - A:MET762	Alkyl
				4.84553	:UNK1:C - A:ARG487	Alkyl
				4.56397	F:DG13 - :UNK1:C	Pi-Alkyl
[XIII]	-9.1	6.658	9.349	2.68138	A:SER464:HG - :UNK1:N	Conventional Hydrogen Bond
				3.02896	F:DG13:H1 - :UNK1:O	Conventional Hydrogen Bond
				3.29478	:UNK1:N - D:DT9:O3'	Conventional Hydrogen Bond
				3.22089	A:ASP463:HN - :UNK1	Pi-Donor Hydrogen Bond
				3.72734	D:DT9:C4' - :UNK1	Pi-Sigma
[XIV]	-9.8	22.870	24.756	2.2727	A:TYR805:HH - :UNK1:N	Conventional Hydrogen Bond
				2.42214	B:LEU616:HN - :UNK1:O	Conventional Hydrogen Bond
				2.03441	B:GLY617:HN - :UNK1:O	Conventional Hydrogen Bond
				3.6969	E:DC8:HO3' - :UNK1:S	Conventional Hydrogen Bond
				1.95633	F:DT9:HOP2 - :UNK1:N	Conventional Hydrogen Bond
				2.52068	:UNK1:H - D:DG13:O6	Conventional Hydrogen Bond
				3.67117	B:GLY760:CA - :UNK1:N	Carbon Hydrogen Bond
				2.90663	A:TYR805:HH - :UNK1	Pi-Donor Hydrogen Bond
				3.6917	:UNK1:C - F:DT9	Pi-Sigma
				3.82937	E:DC8 - :UNK1	Pi-Pi Stacked
				4.8716	:UNK1:C - B:ARG487	Alkyl

Table 6. Results of molecular docking of compounds [XII-XIV] via the human topoisomerase II alpha enzyme

Comp. No.	Affinity (Kcal/mol)	RMSD l.b. (A°)	RMSD u.b. (A°)	Distance (A°)	Main residue	Type of Interaction
doxorobicin	-9.0	3.031	8.702	3.35896	A:SER75:OG - :UNN0:O	Conventional Hydrogen Bond
				2.2511	:UNN0:H - A:SER64:OG	Conventional Hydrogen Bond
				3.5704	:UNN0:C - B:GLY104:O	Carbon Hydrogen Bond
				5.52248	B:PHE63 - :UNN0	Pi-Pi T-shaped
				4.81332	B:PHE63 - :UNN0:C	Pi-Alkyl
				4.93318	:UNN0 - B:ARG66	Pi-Alkyl
				4.68963	:UNN0 - B:ARG66	Pi-Alkyl
				3.35896	A:SER75:OG - :UNN0:O	Conventional Hydrogen Bond

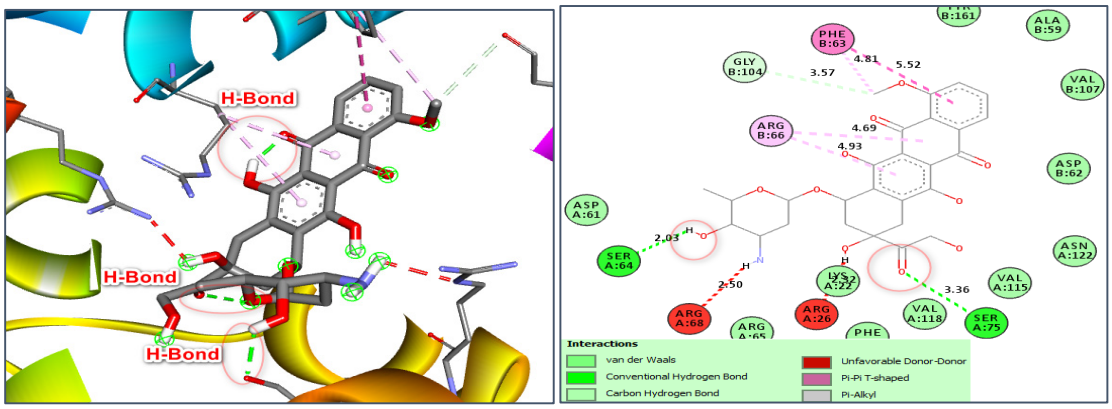

Fig. 7. represents the 2D (right) and 3D (left) structure of the molecular docking of doxorubicin with the binding site of the protein Human topoisomerase IIalpha enzyme (PDB:ID:5GWK)

Fig.8 shows the interaction of compound [XII] at the docking score value equal to -9.5 Kcal/mol and at the conformational value RMSD.i.b(1.493), RMSD.u.b(1.911. The two and three-dimensional cross-sectional images showed the presence of a hydrogen bond between the amino acid residue B: SER:56 with the NH group. In addition to some other bonds, such as a pi-cation and pi-alkyl, as in Table 6.

Molecular docking studies showed compound [XIII] with the protein binding site at the docking point value -9.1 kcal\mol and at the conformational value (RMSD.i.b(5.647), RMSD.u.b(6.865) with the presence of four hydrogen bonds between the amino acid residues GLUB:87, ARG:B:111, GLY:B:163 with a number of OH groups in the compound and the fourth hydrogen bond between The amino acid residues ALA:B:192 are with the NH group, show Fig.9.

Molecular docking studies showed compound [XIV] with the protein binding site at the docking point value -9.8 kcal\mol and at the conformational value (RMSD.i.b(22.870) RMSD.u.b(6.865) with the presence of four hydrogen bonds between the amino acid residues GLUB:87, ARG:B:111, GLY:B:163 with a number of OH groups in the compound and the bond. The fourth hydrogen between the amino acid residues ALA:B:192 with

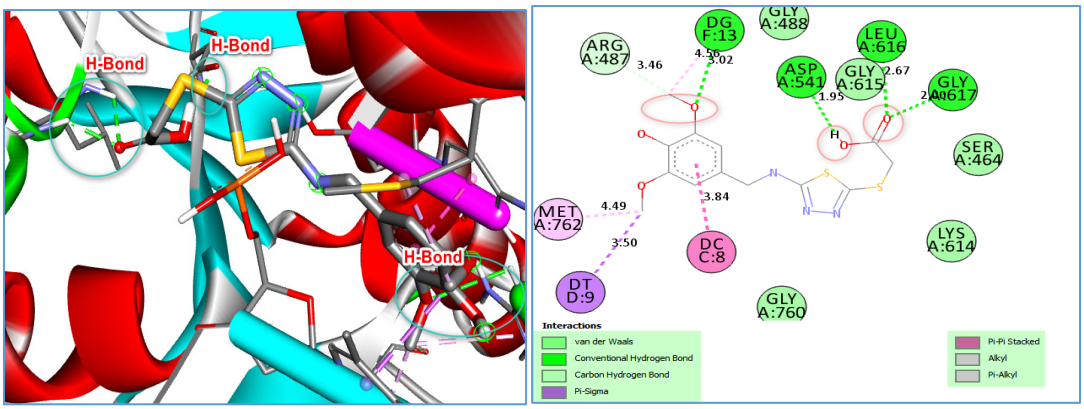

Fig. 8. represents the 2D (right) and 3D (left) structure of the molecular docking of compound [XII] with the binding site of the protein Human topoisomerase IIalpha enzyme (PDB:ID:5GWK)

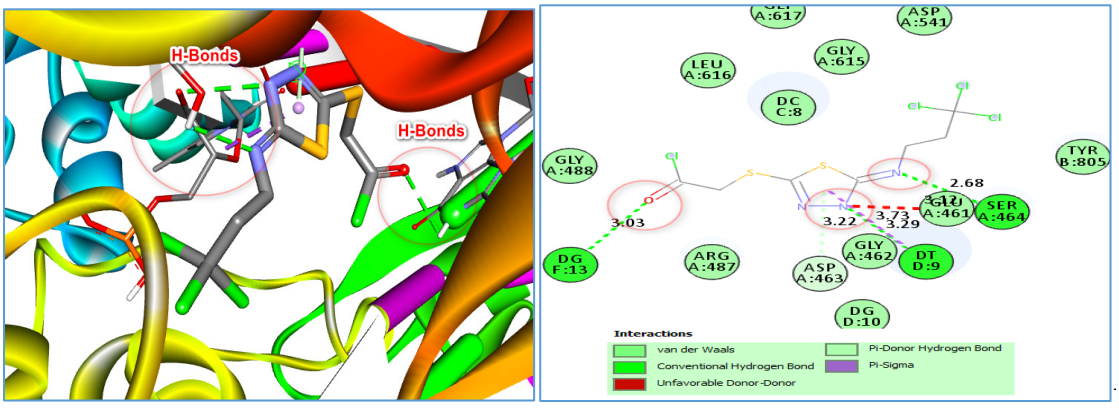

Fig. 9. represents the 2D (right) and 3D (left) structure of the molecular docking of compound [XIII] with the binding site of the protein Human topoisomerase IIalpha enzyme (PDB:ID:5GWK)

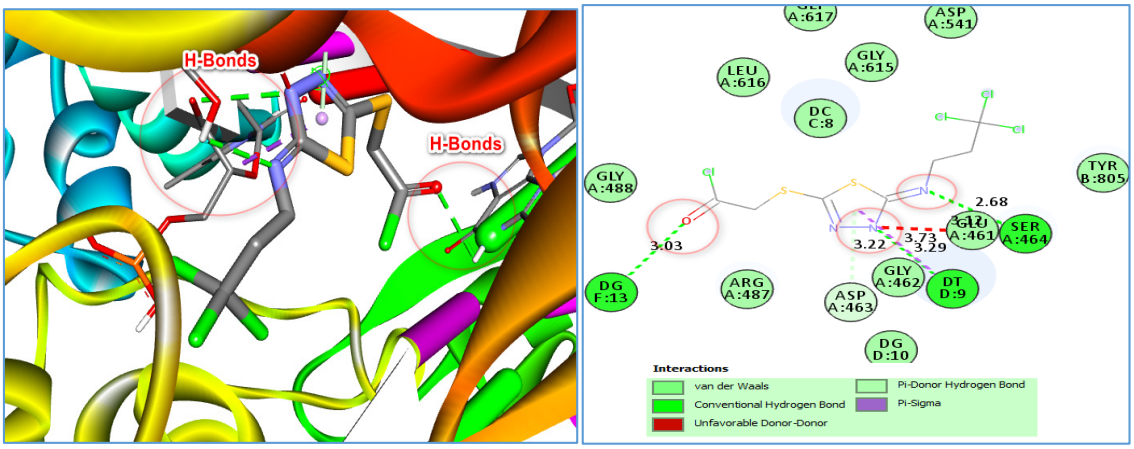

Fig. 10. represents the 2D (right) and 3D (left) structure of the molecular docking of compound [XIV] with the binding site of the protein Human topoisomerase IIalpha enzyme (PDB:ID:5GWK))

the NH group, as shown in the fig.10 and table 6.

From the results obtained above, it is clear that compounds [XII], [XIII]and [XIV] have a better docking score than the drug doxorubicin used as a reference. It also has more hydrogen bonds than the reference, as compound [XII] was linked

to three hydrogen bonds , compound [XIII]to four hydrogen bonds and [XIV] to six hydrogen bonds, while the reference drug was linked to two hydrogen bonds, and the RMSD value appeared lower than the reference drug, which indicates a better match with the binding site.

Biological activity [46,47]

The biological activities of modified CMC [XXIII-XXVI] , modified CMC blended with CS [XXXV-XXXVIII] , polymer blends of CS / modified CMC with gold [XLVI, XLIX] or magnesium [XLVII] or silver [XLVIII] nanocomposites have been tested against two pathogenic bacteria types *(G+) Staphylococcus aureus* and *E. coli (G-)* and compared with two drugs (Amoxicillin ,Tetracycline) and DMSO. The results of antimicrobial activity have been represented in Table 7 and Figures 11-14. The ternary mix (modified CMC/CS) with Au or MgO

Table 7 . Antibacterial screening data of some synthesized polymers and nanocomposites

Comp.No.	*Escharia .coli*	*Staphylococcus aureus*
Amoxicillin	29	11
Tetracycline	12	30
DMSO	Zero	Zero
[XXIII]	22	17
[XXIV]	12	10
[XXV]	13	10
[XXVI]	12	15
[XXXV]	22	23
[XXXVI]	20	22
[XXXVII]	24	25
[XXXVIII]	24	22
[XLVI]	30	31
[XLVII]	28	30
[XLVIII]	28	29
[XLIV]	27	28

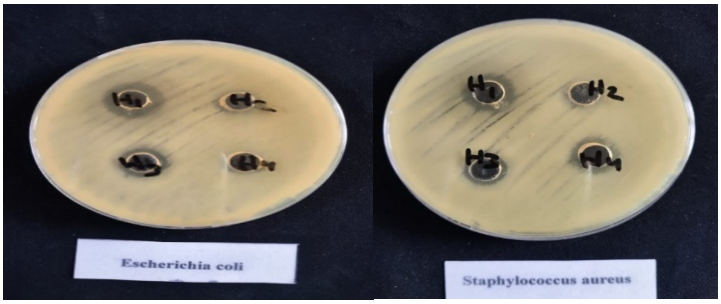

Fig. 11. Antibacterial activities of modified CMC[XXIII-XXVI]

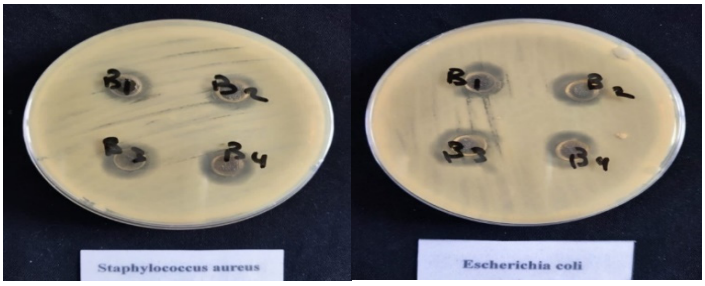

Fig. 12. Antibacterial activities of modified CMC/CS[XXXV-XXXVIII]

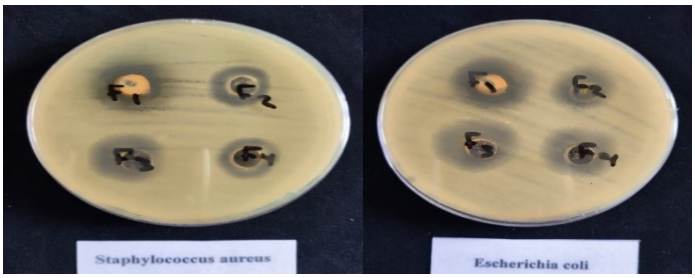

Fig. 13. Antibacterial activities of Nanocomposites[XLVI-XLIX]

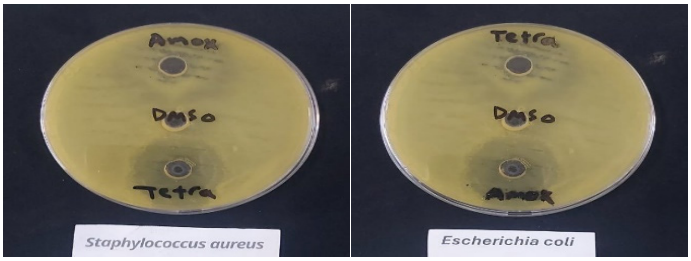

Fig. 14. Antibacterial activities of Amoxicillin, Tetracycline, DMSO

or Ag nanocomposite exhibited good antimicrobial activities comparable with Amoxicillin , Tetracycline as standard antibiotics. The AuNPs have shown excellent antibacterial activities towards *E. coli* through the absorption of the light and converting it to heat. The AuNPs are taken up easily by the immune cells as a result of their excellent cell affinity that results in precise delivery to the infected area, which facilitates the inhibition and the damage to the microbial pathogens. MgONPs was observed that these particles had the capability to generate a notable concentration of active O_2^-. Particularly in acidic or neutral environments, this generation was attributed to the production of hydroperoxyl radicals ($\bullet HO_2$). Furthermore, Ag silver nanocomposite exhibits good antibacterial properties leading to biomedical applications. The antibacterial effect of silver depends on Ag^+, as it binds tightly to electron donor groups in microbial cell walls such as sulphur, nitrogen, or oxygen. However, silver nanoparticles affect bacterial cells by attaching to and entering the bacterial cell wall, and by producing free radicals that can harm the cell and break its membrane.

Antioxidant activity[48,49]

Antioxidants serve as a countermeasure against oxidants. Antioxidants are natural or manmade agents that can inhibit or postpone cellular damage induced by oxidants (ROS, RNS, free radicals, and other unstable chemicals). Halliwell and Gutteridge characterized an antioxidant as any chemical that inhibits, stops, or eliminates oxidative damage to a target molecule. The quantity must be sufficiently high to deactivate the target molecule, necessitating a reaction with oxygen or nitrogen free radicals. No universal antioxidant exists, as distinct antioxidants interact with various reactive substances by diverse methods, at different sites and safeguard specific biochemical targets. The DPPH method was employed to assess the free radical scavenging activity of chemically produced nanocomposites [XLVI, XLVIII]. The DPPH radical scavenging capacity of nanocomposites was compared to that of ascorbic acid. Enhanced outcomes were noted for the synthesized nanocomposites. The nanocomposites demonstrate considerable antioxidant activity and have been utilized in the treatment of disorders induced by oxidative stress. The in vitro antioxidant efficacy of the chosen compounds was assessed by examining their DPPH (2,2-diphenyl-1-picrylhydrazyl) radical scavenging ability in comparison to ascorbic acid,

Table 8. Absorption results and antioxidant activity (RSA%) for the Nanocomposites at different concentrations

Concentrations	H2=modified CMC/CS/AuNPs[XLVI]		H3= modified CMC/CS/AgNPs[XLVIII]		A.A (reference)	
	Abs	RSA%	Abs	RSA%	Abs	RSA%
100 (µg/ml)	0.2	75	0.3	62.5	0.3	**62.5**
80	0.35	56.25	0.32	60	0.33	**58.75**
40	0.43	46.25	0.34	57.5	0.34	**57.5**
20	0.8	28.12	0.36	55	0.4	**50**
10	0.8	20.55	0.4	50	0.52	**35**
DPPH control	0.8					

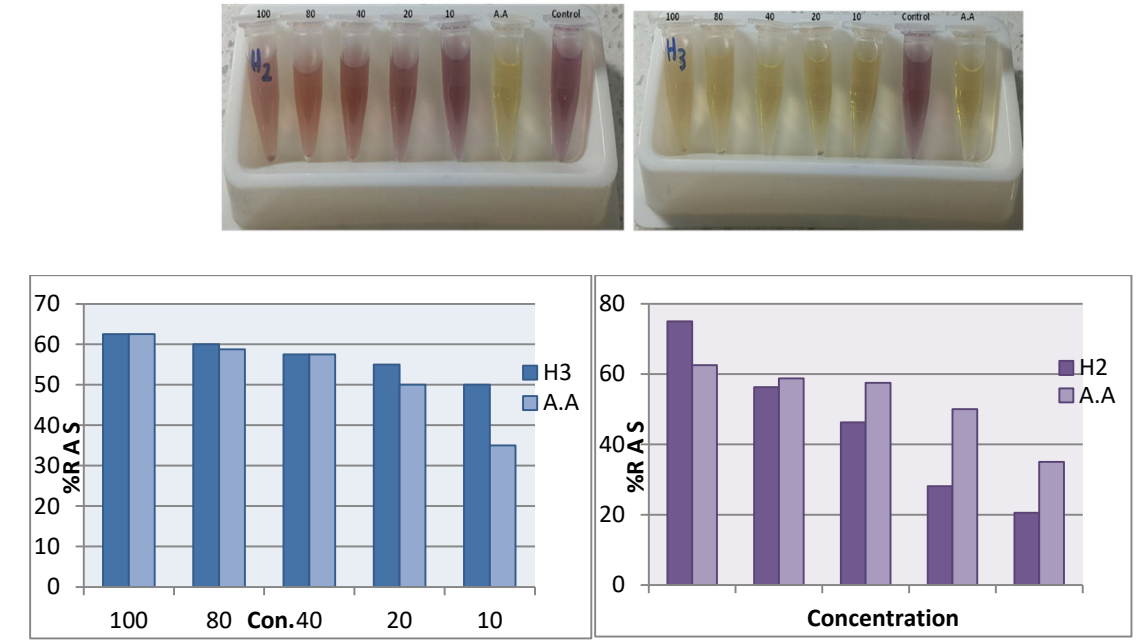

Fig. 15. Testing the antioxidant activity of nanocomposites [XLVI , XLVIII] and comparing with the activity of the reference ascorbic acid compound AA.

a standard antioxidant. The data presented in Table 8, Fig.15, indicate that the nanocomposites exhibit superior activity compared to standard ascorbic acid. The previously stated NH-C=S-nanocomposites exhibited enhanced activity. This is due to a complex group that may absorb and stabilize free radicals through consecutive systems, thereby scavenging them, which then becomes conjugated.

Anticancer activity

Preparation of cell lines for cytotoxicity assays [50] uses grown cells on a 96-well microtiter plate. Absorbance was measured at 620 nm using a microplate reader. The calculated cell growth inhibition rate is defined by the Equation [51]:

Inhibition rate =

$$\frac{mean\ of\ control - mean\ of\ treatment}{mean\ of\ control} \times 100$$

Inhibition rate = (mean of control-mean of treatment)/(mean of control) × 100

The anticancer efficacy of different concentrations of modified CMC/CS [XXXV] and the nanocomposites (modified CMC/CS/AuNPs) [XLVI], (modified CMC/CS/MgONPs) [XLVII] was examined against A172 (human brain cells) and rat embryonic fibroblasts (REF), demonstrating significant activity without impacting the proliferation of normal rat embryonic fibroblasts. Tables 9-12, Fig.16-18 show Nanocomposites [XLVI], [XLVII] demonstrate

Table 9. The inhibition of cell growth after adding various concentrations of blend polymer (Modified CMC/CS [XXXV]

Concen.	A172		REF	
	Mean	SD	Mean	SD
100	58.68	1.97	71.95	0.81
75	65.90	1.77	76.70	2.61
50	71.64	0.42	87.67	3.77
25	83.84	6.21	94.07	5.15
10	86.00	2.14	95.22	0.82

Table 10. The inhibition of cells growth after adding various concentrations of blend polymer (Modified CMC/CS/AuNPs)[XLVI]

Concen.	A172		REF	
	Mean	SD	Mean	SD
100	32.71	2.77	67.94	2.03
75	50.50	2.67	73.15	4.56
50	55.48	1.47	87.58	3.97
25	86.61	2.92	95.56	0.48
10	91.78	0.77	95.60	1.04

Table 11. The inhibition of cells growth after adding various concentrations of nanocomposites (Modified CMC/CS/MgNPs)[XLVII]

Concen.	A172		REF	
	Mean	SD	Mean	SD
100	42.79	2.79	72.65	1.96
75	51.85	3.61	80.21	3.11
50	66.05	2.70	85.65	3.32
25	78.87	10.07	94.17	0.77
10	85.30	1.75	96.18	0.23

Table 12. IC50 (Inhibitor Concentration Fifty) of blend polymer and nanocomposites

Treatment	IC_{50} in µg/Ml	
	A172	REF
Modified CMC/CS[XXXV]	110.1	92.55
ModifiedCMC/CS/AuNPs[XLVI]	81.94	42.19
ModifiedCMC/CS/MgNPs[XLVII]	125.7	60.22

superior inhibition compared to the polymer blend [XXXV]. It is essential to further investigate the mechanisms by which nano and heterocyclic units exert powerful cytotoxic effects, which may render chitosan derivatives promising candidates for anti-cancer medications. AuNPs, MgONPs demonstrate significant cytotoxicity. A dose-dependent increase in the activation of apoptosis and reactive oxygen species production. Bio-synthesized metal nanoparticles, particularly gold, magnesium, and their conjugates with biopolymers, possess significant potential across various scientific domains due to their extensive variety of applications, including biomedical uses.

Acute Toxicity Test [52-55]

This investigation was carried out at the laboratory of the Centre for Cancer Research and Medical Genetics to assess the acute toxicity of certain synthesized polymer nanocomposites, employing the Lorke method. The study involved (25) laboratory albino mice, aged three months, with average weights ranging from (20-26) grams, all of which were male. These animals were housed in plastic cages with metal lids, coated with fine sawdust, and provided with water via plastic bottles,

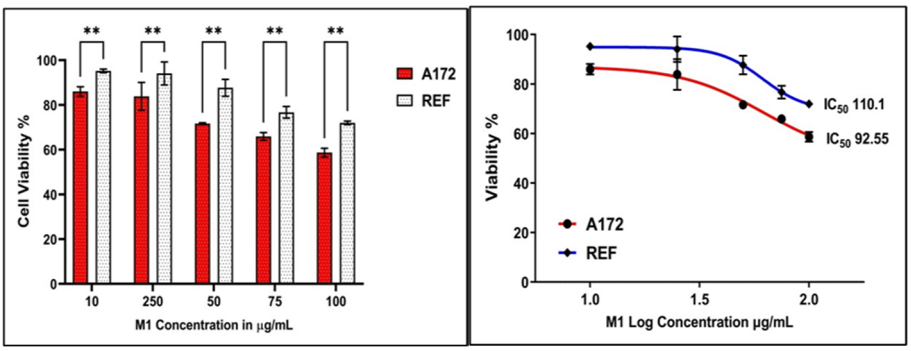

Fig. 16. Cell Viability and IC50 of M1 (modified CMC/CS)[XXXV]on A172 and compare with REF

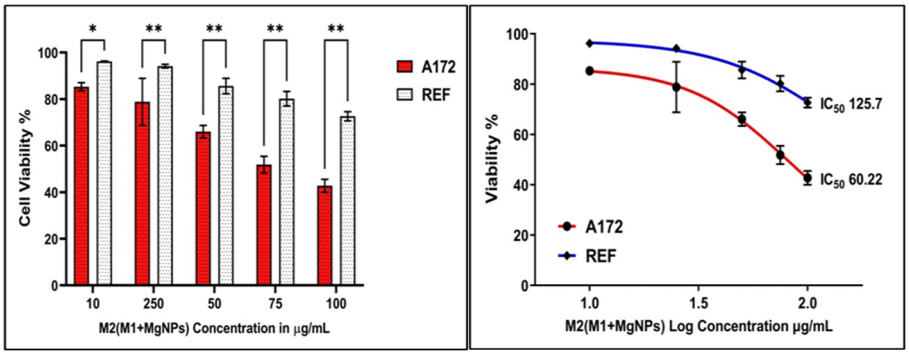

Fig. 17. Cell Viability and IC50 of M2 (modified CMC/CS/Mg)[XLVII]on A172and compare with REF

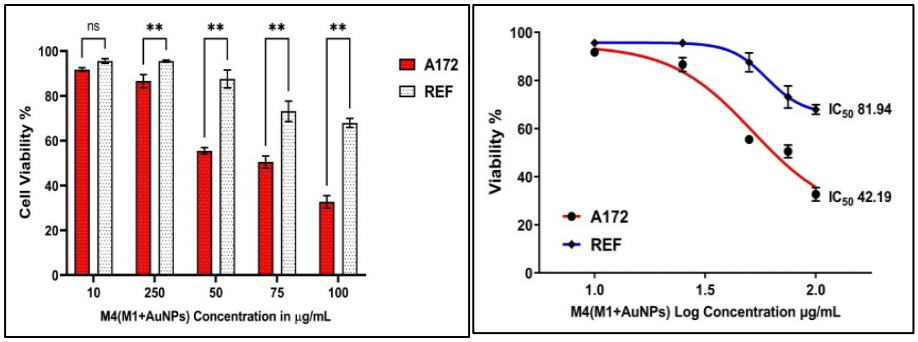

Fig. 18 .Cell Viability and IC50 of M4 (modified CMC/CS/Au)[XLVI] on A172and compare with REF

along with food supplies. Mice were subjected to an 18-hour fasting period with unrestricted access to water and food before the test. The compounds were dissolved in distilled water and subsequently administered via injection at dosages of (5 g/kg and 10g/kg). The treatment group and the control group were evaluated based on injection dosages, revealing after (14) days: no mortality at (5 g/kg and 10g/kg) body weight doses, no significant differences in daily weight measurements between the control and treatment groups, no alterations in mouse behavior, and no reported symptoms of toxicity. Furthermore, several mice have been euthanized via cervical dislocation, and the liver, kidneys, heart, and lungs have been weighed. The visual assessment of murine organs exhibited a normal appearance. These results suggested that polymer nanocomposites have low toxicity towards both examined organisms.

Histological Study

Histological examination of the liver, kidney,

Fig.19. Image of mice: in plastic cages, during injection

Fig. 20. A section of liver (control) shows a normal central vein (V) & normally hepatocytes (h) & normal sinusoid (S). H&E.400x

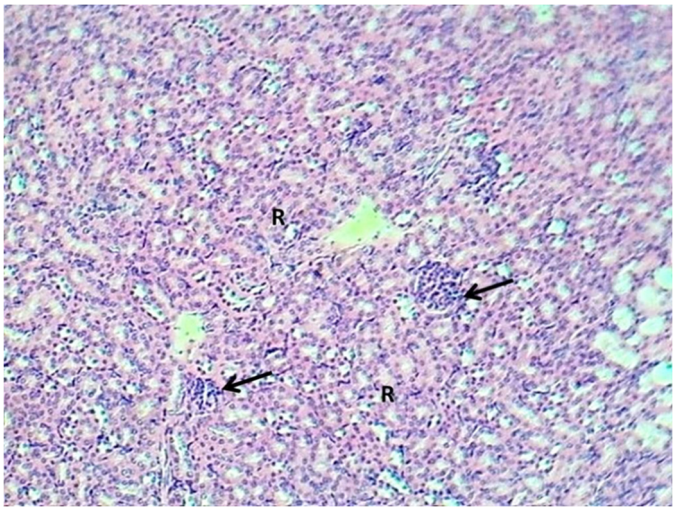

Fig. 21. Section of renal cortex of control shows normal lining cells of renal tubules (R), & normal glomeruli (arrows). H&E.100x

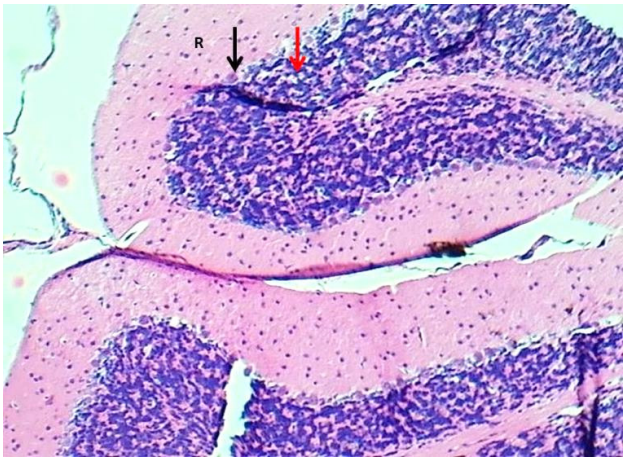

Fig. 22. Section of cerebellum (control) shows normal appearance reticular layer (R), normal layer of purkinji cells (black arrow) & normal granular layer (red arrow) . H&E.100x

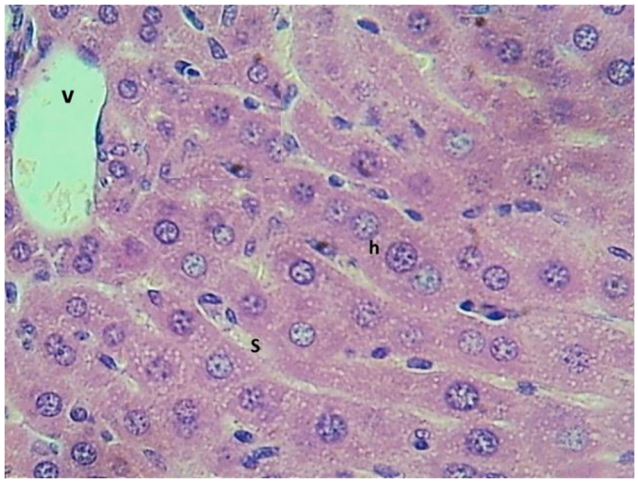

Fig. 23. Section of liver (after injecting it with nanocomposites) shows normal sinusoid (S), normal hepatocyte (h) & central vein (v). H&E.400x

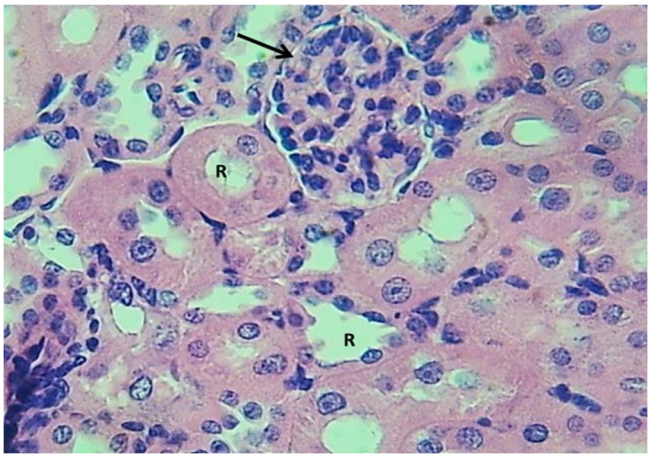

Fig. 24. section of renal cortex (after injecting it with nanocomposites) shows normal glomeruli (Arrows) with normal renal tubules (R). H&E.100x

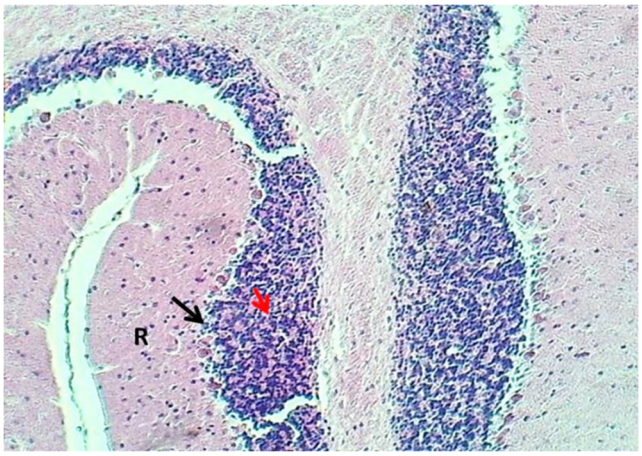

Fig. 25. section of cerebellum (after injecting it with nanocomposites) shows normal appearance of cerebellar layers and cells (1&2). H&E.100x

and brain related to the treated group showed no changes but similarities to those of the control group.

CONCLUSION

In this study, the synthesis, characterization and study of molecular docking, antibacterial, antioxidant and anticancer activities of some new modified CMC containing chitosan and nanoparticles such as gold nanoparticles, magnesium oxide nanoparticles and silver nanoparticles. TEM and FESEM studies showed the changes in the surface morphology of the synthesized polymers due to the new bonds between chitosan and modified CMC and nanoparticles. Results have indicated that nanocomposites had a greater diameter of the growth inhibition zone compared to standard antibiotics (amoxicillin, tetracycline). Finally, the antioxidant activity of modified CMC/CS/NPs exhibited a high inhibition rate compared to standard ascorbic acid. MTT assay was used to estimate the cytotoxic effect of different concentrations of the created nanocomposites for the cancer cell line (A172) and compare with the normal cell line (REF); the nanocomposites exhibited a very excellent inhibition rate. Finally, toxicity tests and histological studies for these nanocomposites are conducted, where it showed the non-toxicity of these nanocomposites.

ACKNOWLEDGEMENT

The authors thank the Dean of the College, the Head of the Department, and the professors working in the scientific laboratories for their continuous support throughout the research.

ETHICAL APPROVAL

we affirm that our submitted manuscript adheres to the ethical guidelines outlined above regarding the use of animals in research.

AUTHORS' DECLARATION

Conflicts of Interest: None. We hereby confirm that all the Figures and Tables in the manuscript are ours. Furthermore, any Figures and images, that are not ours, have been included with the necessary permission for republication, which is attached to the manuscript. Ethical Clearance: The project was approved by the local ethical committee at University of Baghdad

AUTHORS' CONTRIBUTION STATEMENT

Study conception and design: Ruwaidah S.Saeed; data collection: Huda H.Saeed; analysis and interpretation of results: Huda H.Saeed , Ruwaidah S.Saeed and Lyazzat Bekbayeva; draft manuscript preparation: Lyazzat Bekbayeva. All authors reviewed the results and approved the final version of the manuscript.

REFERENCES

1. Ariffin Adi Hafizamri A, Wan Mohd Norsani WN, Samsuri A, Mohd Ikmar Nizam MI, Vincent I, Mohammad Fakhratul RZ. Corrosion Inhibition Study of Carboxymethyl cellulose Ionic Liquid Via Electrochemical and Machine Learning Technique. Malays J Anal Sci. 2024;28(2):265-76.

2. Yao X, Qian D, Changqing R, Dan X, Kaifang Z. Application of Carboxymethyl Cellulose and Its Edible Composite Coating in Fruit Preservation. Packag Technol Sci. 2024;37(8):781-92. https://doi.org/10.1002/pts.2822
3. Stephan S. Evaluation of Carboxymethyl Cellulose as an Additive for Selective Protein Removal from Wine. Fermentation. 2025;11(5):273. https://doi.org/10.3390/fermentation11050273
4. Zahra S, Hadi B, Najmeh N, Kamyar K. Evaluation of Carboxymethyl Cellulose/Gelatin Hydrogel-Based Dressing Containing Cefdinir for Wound Healing Promotion in Animal Model. Gels. 2025;11(1):38. https://doi.org/10.3390/gels11010038
5. Aditi A, Janarthanan R, Ajitkumar G, Dattatray P, Akhilesh Sh. Effectiveness and safety of carboxymethyl cellulose eye drops in dry eye disease: A real-world study. Natl J Physiol Pharm Pharmacol. 2025;15(1):114-8. https://doi.org/10.5455/NJPPP.2025.v15.i1.20
6. Nurul Athirah SMZ, Kelvin Ng, Bee CA. Fabrication of water-stable soy protein isolate (SPI)/ carboxymethyl cellulose (CMC) scaffold sourced from oil palm empty fruit bunch (OPEFB) for bone tissue engineering. Ind Crops Prod. 2025;224:120325. https://doi.org/10.1016/j.indcrop.2024.120325
7. Wen-Hsin H, Chia-Yi H, Pao-Chang C, Hsiang L, Ting L, Pin-Chuang L, et al. Physicochemical Characterization, Biocompatibility, and Antibacterial Properties of CMC/PVA/Calendula officinalis Films for Biomedical Applications. Polymers (Basel). 2023;15(6):1454. https://doi.org/10.3390/polym15061454
8. Parvinder K, Tanweer A, Harinder S, Jyoti J, Gayatri S, Broadway AA. Organic Acids Modified Starch-CMC Based Biodegradable Film: Antibacterial Activity, Morphological, Structural, Thermal, and Crystalline Properties. J Pure Appl Microbiol. 2023;17(1):241-57. https://doi.org/10.22207/JPAM.17.1.14
9. El-naggar AM, Lamya AA, Kamal AM, Albassam AA, Lakshminarayana G, Mohamed BM. Polyvinyl alcohol/carboxymethyl cellulose blended polymers doped with PPy/milled MWCNTs filler for Flexible optoelectronic and Energy Storage Applications. Polym Test. 2024;138:108551. https://doi.org/10.1016/j.polymertesting.2024.108551
10. Shengkai L, Huiling L, Xi L, Wei W, Chunguang R, Mengjie Y, et al. PVA-enhanced green synthesis of CMC-based lithium adsorption films. Carbohydr Polym. 2025;349(Pt A):122973. https://doi.org/10.1016/j.carbpol.2024.122973
11. Salem SS, Amr HH, Al-Aliaa MS, Ahmed SD, Amr AA, Amr MS. Synthesis of Silver Nanocomposite Based on Carboxymethyl Cellulose: Antibacterial, Antifungal and Anticancer Activities. Polymers (Basel). 2022;14(16):3352. https://doi.org/10.3390/polym14163352
12. Yassin AY, Abdelghany AM, Reda SS, Tarabiah AE. Structural, Optical and Antibacterial Activity Studies on CMC/PVA Blend Filled with Three Different Types of Green Synthesized ZnO Nanoparticles. J Inorg Organomet Polym Mater. 2023;33:1855-67. https://doi.org/10.1007/s10904-023-02622-y
13. Enes A, Abdulbaki B, Murat K. Carboxymethyl Cellulose (CMC)-Reinforced Polyvinyl Alcohol (PVA) Fibrillar Composite Membranes: Production by Centrifugal Spinning and Characterization. Adv Polym Technol. 2025;2025:1-11. https://doi.org/10.1155/adv/2382763
14. Javier MAM, Vanessa FS, Angela YBL, Marcos LD, Rossana MSM. Spinnability and Morphological Stability of Carboxymethyl Cellulose and Poly(Vinyl Alcohol) Blends by Electrospinning. Processes. 2024;12(12):2759. https://doi.org/10.3390/pr12122759
15. Widad HA, Mustafa HS, Mustafa ZA. Enhancing Structural and Optical Properties of PVA: CMC Blend by NiO Nanoparticle. J Nanostruct. 2025;15(2):459-66.
16. Abdelghany AM, Nuha YE, Younis Sh, Ayaad DM. Polyvinyl pyrrolidone/ carboxymethyl cellulose (PVP/CMC) polymer composites containing CuO nanoparticles synthesized via laser ablation in liquids. J Mol Liq. 2024;403:124857. https://doi.org/10.1016/j.molliq.2024.124857
17. Maida A, Hassan M, Maliha U, Ayesha IA. Comparative Study of Different Methods for Cellulose Extraction from Lignocellulosic Wastes and Conversion into Carboxymethyl Cellulose. ChemistrySelect. 2022;7(29):e202201533. https://doi.org/10.1002/slct.202201533
18. Sun Theo CLN, Anita M, Bangun SN, Edi P, Qolby S, Evi YI, et al. Preparation and characterization of polymer blend electrolyte membranes based on lithium acetate-complexed carboxymethyl cellulose (CMC) and carboxymethyl chitosan (CMCh) blend. Polym Eng Sci. 2024;64(2):761-78. https://doi.org/10.1002/pen.26582
19. Doaa Elsayed M, Nashiru B. Physicochemical modifications in microwave-irradiated chitosan: biopharmaceutical and medical applications. J Biomater Sci Polym Ed. 2024;35(6):898-915. https://doi.org/10.1080/09205063.2024.2306695
20. Ujjwal KB, Anindya B, Bhavna G, Susrita S. An insight into chemically modified chitosan and their biological, pharmaceutical, and medical applications: A review. Int J Biol Macromol. 2025;303:140612. https://doi.org/10.1016/j.ijbiomac.2025.140612
21. Weronika K, Karol KK, Katarzyna HG, Piotr G, Mateusz K, ˙Zaneta KK, et al. Review: Medical Applications and Cellular Mechanisms of Action of Carboxymethyl Chitosan Hydrogels. Molecules. 2024;29(18):4360. https://doi.org/10.3390/molecules29184360
22. Vijaya K, Mayuri P, Sakshi K, Sanyog P, Devashish N, Sohani S. Chitosan as a sustainable biopolymer: A comprehensive review. J Pharmacogn Phytochem. 2025;14(2):102-7. https://doi.org/10.22271/phyto.2025.v14.i2b.15280
23. Ahmed GT, Mohammed FR, Mohamed EA, Nada MA, Mohamed RE. Green Synthesis and Applications of Modified Schiff Base Chitosan Derivative. Afr J

Biomed Res. 2024;27(4s):58-64.
24. Lijie L, Muhammad IB, Wiebe MV, Saskia L. Preparation of Sodium Carboxymethyl Cellulose-Chitosan Complex Membranes through Sustainable Aqueous Phase Separation. ACS Appl Polym Mater. 2023;5(3):1810-8. https://doi.org/10.1021/acsapm.2c01901
25. Mengya Li, Haofan Qu, Qin Li, Shengchang Lu, Yang Wu, Zuwu Tang, et al. A carboxymethyl cellulose/chitosan-based hydrogel harvests robust adhesive, on-demand detachment and self-healing performances for deep burn healing. Chem Eng J. 2024;498:155552. https://doi.org/10.1016/j.cej.2024.155552
26. Maria M, Sara BS, Raquel M, Jo˜ao Paulo F, Sandra B, Manuela P. Exploring the potential of mealworm chitosan for hemodialysis applications. Sustain Chem Pharm. 2025;45:102013. https://doi.org/10.1016/j.scp.2025.102013
27. Ruwaidah SS. Synthesis and Characterization of O-(carboxyl) Chitosan Schiff Base Derivatives and Study Antibacterial Activity. Int J Drug Deliv Technol. 2020;10(3):402-7. https://doi.org/10.25258/ijddt.10.3.17
28. Marwa H, Haozhi S, Lixia P, Dandan W, Mengxiao S, Zhaoning Z, et al. Chitosan and its derivatives as potential biomaterials for biomedical and pharmaceutical applications: A comprehensive review on green extraction approaches, recent progresses, and perspectives. Eur Polym J. 2025;229:113882. https://doi.org/10.1016/j.eurpolymj.2025.113882
29. Dominika Ž, Veronika M, Peter M. Advances in Chitosan Derivatives: Preparation, Properties and Applications in Pharmacy and Medicine. Gels. 2024;10(11):701. https://doi.org/10.3390/gels10110701
30. Ebrahim C, Zahra C. Chitosan: A Comprehensive Review of Structural Properties, Biological Activities, and Multidisciplinary Applications. Curr Trends Biotechnol Pharm. 2025;19(2):2372-85. https://doi.org/10.5530/ctbp.2025.2.23
31. Emir A, Hatice D, Furkan E, Mikhael B, Sercan K. Chitosan and Its Nanoparticles: A Multifaceted Approach to Antibacterial Applications. J Nanomater. 2025;15(2):126. https://doi.org/10.3390/nano15020126
32. YAN Q, WEI P, PENG R, TIAN S, LI D, TONG Y, et al. Controllable Synthesis of Carboxymethyl Cellulose and Its Application in Tobacco Sheets. Wuhan Univ J Nat Sci. 2023;28(4):341-50. https://doi.org/10.1051/wujns/2023284341
33. Ali HS, Khalid FA, Ruwaidah SS. Synthesis and Characterization of Some New Thiazine, Azetidine and Thiazolidine Compounds Containing 1,3,4-Thiadiazole Moiety And Their Antibacterial Study. Ibn Al-Haitham J Pure Appl Sci. 2014;27(3):350-64.
34. Saeed RS, Al-Rawi MS. Synthesis, Characterization, Study the Toxicity and Anticancer Activity of N,O-Chitosan Derivatives. Int J Pharm Res. 2020;12(2):297-304. https://doi.org/10.31838/ijpr/2020.12.02.0180
35. Shrba HA, Hassan AH, Ali FK. Synthesis and Characterization of New Azo Compounds Derived from 4-Amino Acetophenone and Studying their Liquid Crystal Behavior. Int J Sci Technol. 2013;8(2):55-61.
36. Fouad MS, Redha I, Al-Bagat, Araa Al-Juboori. Synthesis and Characterization of New Azo Compounds Derived from 2-Amino Benzimidazole. Al-Mustansiriya J Sci. 2006;17(3):15-26.
37. Kareem AF, Thejeel KA, Mohammed Ali IA, Alrawi MS, Abdullah RG. Synthesis and Study Antimicrobial/Antioxidant of Some New Derivatives Derived from Drug Levofloxacin. Adv J Chem A. 2024;7(6):677-86.
38. Kunal P, Banthia AK, Majumdar DK. Esterification of Carboxymethyl Cellulose with Acrylic Acid for Targeted Drug Delivery System. Trends Biomater Artif Organs. 2025;19(1):12-4.
39. Widad AS, Saeed RS. Gold and Silver Nanoparticles with Modified Chitosan /PVA: Synthesis, Study The Toxicity and Anticancer Activity. Nanomed Res J. 2023;8(3):231-45.
40. Mehrab P, Erfan R, Amin S, Amirmasoud S, Javad E, Rabia A, et al. Novel carboxymethyl cellulose based nanocomposite: A promising biomaterial for biomedical applications. Process Biochem. 2023;130:211-26. https://doi.org/10.1016/j.procbio.2023.03.033
41. Mohammed Yassen T, Marouf AL-Azzawi A. Synthesis and Characterization of New Bis-Schiff Bases Linked to Various Imide Cycles. Iraqi J Sci. 2023;64(3):1062-70. https://doi.org/10.24996/ijs.2023.64.3.3
42. Abdul wahid Abdul-Zahra M, Abbass NM. Synthesis and Characterization of Nano-Composites of Polypropylene / Cr2O3 Nanoparticles Using Licorice Extract. Iraqi J Sci. 2024;65(2):623-63. https://doi.org/10.24996/ijs.2024.65.2.4
43. Asaad Noora, Ismaeel Y. Majeed, Ahmed Ahmed, Alabdullah Sahar S. Microwave synthesis, density functional theory study and antiproliferative activity of the novel spiropyrazole derivatives. Results Chem. 2024;11:101758. https://doi.org/10.1016/j.rechem.2024.101758
44. Saeed RS, Attiya HG, Obead KA. Synthesis and Characterization of Grafted Chitosan Blending with Polyvinyl alcohol / Nanocomposite and Study Biological Activity. Baghdad Sci J. 2023;20(5):1692-700. https://doi.org/10.21123/bsj.2023.7574
45. Sabah AA, Mhaibes RM, Jarallah AL, Salman SD, Al-Rawi MS. Study the Toxicity and Anticancer Activity of Some New Derivatives of Mefenamic Acid. J Med Chem Sci. 2023;6(5):1000-9.
46. Nayyef Rasha Shakere, Awad, Sana Hitur. Synthesis and characterization of new derivatives of CMC-g-PVA and evaluation pharmaceutical release, antibacterial activity, molecular docking. J Neonatal Surg. 2025;14(4s):675-87. https://doi.org/10.52783/jns.v14.1861
47. Saeed RS, Matty FS, Samir AH, Al-Rawi MS. Synthesis, characterization and antibacterial study of selected metal complexes derived from modified of PVA. J Glob Pharm Technol. 2019;11(2):108-17.
48. Al-Majidi MH, Al-Khuzaie MGA. Synthesis and Characterization of New Azo Compounds Linked

to 1,8-Naphthalimide and Studying Their Ability as Acid-Base Indicators. Iraqi J Sci. 2019;60(11):2341-52. https://doi.org/10.24996/ijs.2019.60.11.4
49. Al-Rawi MS. Synthesis of some new heterocyclic compounds via chalcone derivatives. Ibn Al-Haitham J Pure Appl Sci. 2015;28(1):88-99.
50. Freshney RI. Culture of Animal Cells: A manual of Basic Technique and Specialized Applications. 6th ed. New York: Wiley; 2010. https://doi.org/10.1002/9780470649367
51. Gao S, Ya BP, Dong WG, Luo HS. Antiproliferative effect of octreotide on gastric cancer cells mediated by inhibition of Akt/PKB and telomerase. World J Gastroenterol. 2003;9(10):2362-5. https://doi.org/10.3748/wjg.v9.i10.2362
52. Mikhailova EO. Gold Nanoparticles: Biosynthesis and Potential of Biomedical Application. J Funct Biomater. 2021;12(4):70. https://doi.org/10.3390/jfb12040070
53. Hanane M. Cytotoxicity of the Aqueous Extract and Organic Fractions from Origanum majorana on Human Breast Cell Line MDA-MB-231 and Human Colon Cell Line HT-29. Adv Pharmacol Sci. 2018;2018:3287193. https://doi.org/10.1155/2018/3297193
54. Aké-Assi E, N'guessan K, Kouassi AF. Evaluation de la toxicité aiguë de l'extrait aqueux des feuilles de Thunbergia atacorensis, une espèce nouvelle. Eur Sci J. 2015;11(27):92-100.
55. Saeed RS, Hassan HA, AL-Rawi MS. Modification and Study Biological Activity of Chitosan with Compounds Containing Azo Group. Baghdad Sci J. 2025;22(2):428-37. https://doi.org/10.21123/bsj.2024.9453